Excited State Structure Correlates with Efficient Photoconversion in Unidirectional Motors

Palas Roy,[1] Andy S. Sardjan,[2] Arjen Cnossen,[2] Wesley R. Browne,[2] Ben L. Feringa,[2] and Stephen R. Meech[1]**

[1] School of Chemistry, University of East Anglia, Norwich Research Park, Norwich NR4 7TJ, U.K. [2] Stratingh Institute for Chemistry, University of Groningen, Nijenborgh 4, 9747AG Groningen, The Netherlands.

Corresponding Authors

* s.meech@uea.ac.uk; b.l.feringa@rug.nl

ABSTRACT. The design of unidirectional photomolecular motors demands a critical understanding of an ultrafast photochemical isomerisation. An intermediate dark excited state mediates the reaction via a conical intersection (CI) with the ground state, but a correlation between molecular structure and photoisomerisation efficiency remained elusive. Here femtosecond stimulated Raman spectroscopy captures vibrational spectra of the dark state in a set of molecular motors bearing different substituents. A direct correlation between isomerization quantum yield, dark state lifetime and excited state vibrational spectrum is found. Electron withdrawing substituents lead to activity in lower frequency modes, which we correlate with a pyramidalization distortion at the ethylenic axle occurring within 100 fs. This structure is not formed with an electron donating substituent, where the axle retains double bond character. Further structural reorganization is observed and assigned to excited state reorganization and charge redistribution on the sub-ps time scale. The correlation of dark state structure with photoconversion performance suggests guidelines for developing new more efficient motor derivatives.

TOC GRAPHICS

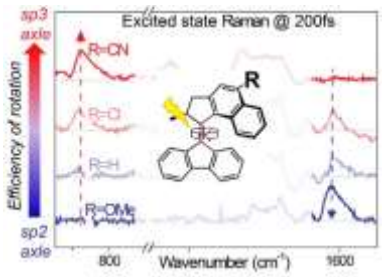

KEYWORDS. Ultrafast, Femtosecond stimulated Raman, light driven molecular motor, excited state, transient absorption, conical intersection.

Artificial unidirectional photochemically driven motors are a powerful tool for generating mechanical energy on a molecular scale by absorption of light.[1-4] They have been used in a wide range of applications from ultrafast responsive materials to catalysis.[5-8] The basis of their function is a photochemical cis-trans isomerization in a sterically overcrowded alkene, which facilitates unidirectional rotation of the motor.[9-12] Second generation motors with a 'stator' fluorene ring linked to a 'rotor' moiety through a double bond 'axle' (Figure 1) have the fastest rates of rotation.[9] A schematic of their operation is shown in Figure 1. The first step involves photo-isomerization around the alkene axle, giving rise to a metastable ground state with a yield of 5-20% depending upon the substituent.[13] The second step is a thermally activated helix inversion to complete a 180 degree rotation.[2, 14] The process is repeated with a second photon absorption and thermalization step to drive a full cycle rotation. Thus, the thermal step is rate limiting while the photochemical step determines the quantum yield.

The photochemical step has been studied theoretically and shown to involve ultrafast structural dynamics in the excited state leading to a conical intersection (CI) with the electronic ground state, from which either the isomerized metastable product or the original state may be generated.[15-16] The corresponding potential energy diagram is shown in Figure 1 (top). However, exploitation of these second generation motors may be limited by the relatively low yield of the photochemical isomerization. This has prompted investigations of the effects of variation in substituent and structure, with the aim of maximizing photoisomerization efficiency.[17-20] However, the development of predictive models for future syntheses certainly requires a detailed understanding of the effects of such structural modifications on excited state dynamics. For example, Filatov and Olivucci have shown theoretically that substituents significantly modify the

pathway of structural evolution near the CIs connecting ground and excited states, thus modifying the photochemical yield.[21]

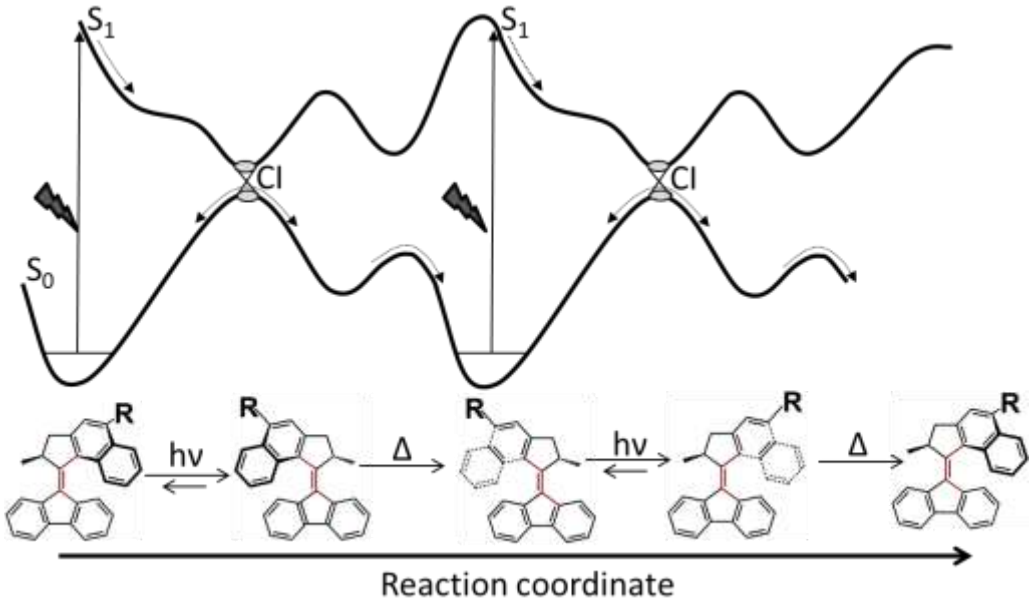

Figure 1: The dynamics of a light-driven molecular motor. Structure of the molecular motor, the steps in its photoconversion mechanism and a schematic of the corresponding potential energy surface. The ground and excited state potential energy surfaces intersect at the conical intersection, CI. (R = H, OMe, Cl, CN)

Earlier experimental studies of excited state dynamics in second generation motors used ultrafast fluorescence spectroscopy to probe the primary photochemical step. A relaxation of the Franck-Condon (FC) bright state occurs in about 100 fs populating an intermediate 'dark state' on the excited state surface.[22] Extending those studies to a series of substituted second generation motors showed that the energetics and lifetime of the dark state are a function of the substituent, which also modified the photoconversion efficiency, with the yield increasing with increasing substituent electron withdrawing character (CN = 0.2, Cl = 0.15, H = 0.14, OMe = 0.05).[13] The

weak dependence of bright state lifetime on solvent viscosity, coupled with the results of computational calculations, suggested pyramidalisation at an axle C atom as an important coordinate in the excited state structural dynamics.[13, 15-16, 22] However, direct experimental evidence for the role of a pyramidalisation coordinate in dark state formation and decay has not been provided to date.

Here we report a structure-function correlation between Raman spectra of the dark excited state and photoconversion efficiency in a series of substituted molecular motors. Specifically, we have measured ground and ultrafast excited state Raman spectra in four derivatives of the fluorene molecular motor 9-(2-methyl-2,3-dihydro-1H-cyclopenta[a]naphthalen-1-ylidene)-9H-fluorene, with substituents (−R): −H, electron withdrawing groups (–CN and –Cl), and electron donating group (–OMe). We find remarkable differences in dark state vibrational spectra for these four molecules, with specific Raman active modes swapping their relative intensities as a function of substituent. We assign this to substituent control of the dark state structure in the four derivatives. Further structural evolution in the dark state is also resolved.

Steady state measurements: Steady-state absorption spectra for the four motor derivatives in methanol are shown in SI Figure S1. The absorption maxima for R = OMe, H, Cl and CN derivatives are at 402, 387, 391 and 402 nm respectively, corresponding to a π-π^* transition. Quantum chemical calculations reveal that this transition is localized on the ethylenic axle of the motor.[23] Thus, the observed spectral shifts indicate that the peripheral substituents affect the electronic structure at the core of the molecule.

In order to better understand the effect of substituent on ground state structure, we recorded steady-state Raman spectra under non-resonant conditions at 532 nm (Figure 2). The strongest

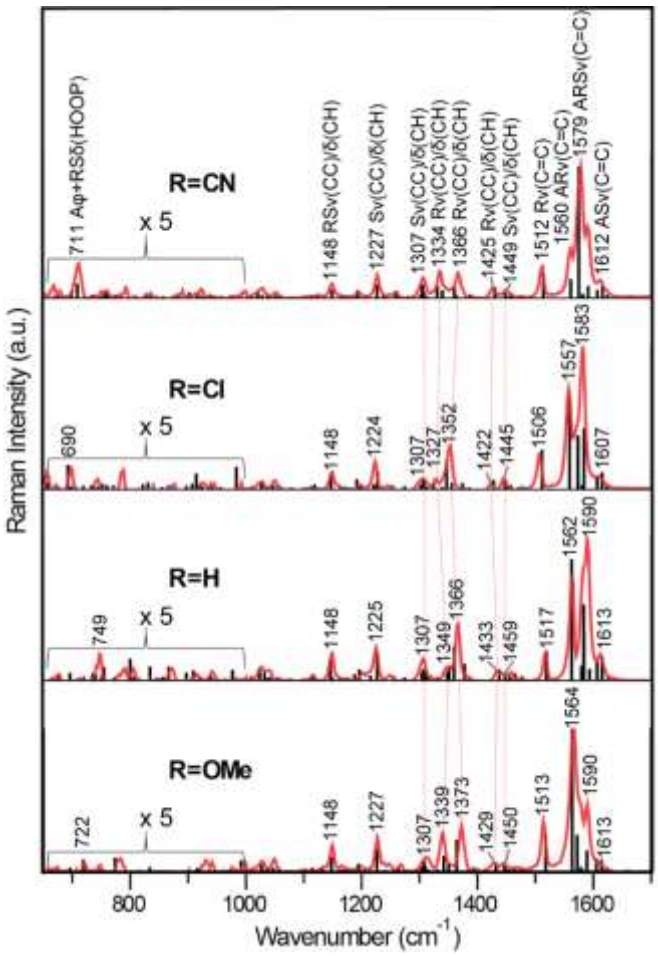

Figure 2: Experimental (red solid lines) and calculated (black vertical lines) steady-state off-resonance (or pre-resonance) Raman of the four motor derivatives in the solid state. Raman at 532 nm, resonance wavelength ca 400 nm. The region 650-1000 cm^{-1} is increased by a factor of 5 to show the weak spectral features more clearly. The peaks in the region 1300-1400 cm^{-1} are connected by red dotted lines to show substituent dependence. The symbols represent υ- stretching, δ- bending, φ- pyramidalisation, A- ethylenic Axle, R- substituted naphthyl Rotor and S- fluorene Stator.

Raman active mode in all four derivatives is in the region of 1500-1600 cm^{-1}. The finger print region (1300-1500 cm^{-1}) shows significant variation, with the substituent dependence of modes

of the same character being highlighted by red dotted lines. This variation indicates an effect of substituent on the Raman active modes of the naphthyl unit to which the substituents are attached (see below). The region 1100-1250 cm^{-1} is again quite similar for all four derivatives, while activity in low frequency modes (<1000 cm^{-1}) is very weak in all cases, although there is moderate intensity in a mode near 750 cm^{-1}.

Ground-state DFT calculations of Raman active modes using Gaussian16 were used to assign these spectra; calculated data (at the rb3lyp/tzvp level, frequency scaled by 0.98) are shown by black vertical lines in Figure 2. The experimental and calculated spectra match quite well for all the derivatives in the region 650-1700 cm^{-1}. The modes near 1580 cm^{-1} arise from symmetric stretching of the ethylenic C=C axle coupled to ring breathing modes (υ(C=C)), while the finger-print region from 1100-1500 cm^{-1} is dominated by stretching (υ(CC)) and bending (δ(CH)) modes of both the rotor (naphthyl) and stator (fluorene) groups. The character of the most prominent modes are labelled in Figure 2 and their nuclear displacements are illustrated in SI, Figure S4. The modes with a significant substituent dependence (shown by the red dotted lines) are seen to arise from ring υ(CC)/δ(CH) modes of the naphthyl rotor bearing the substituent. The peak frequencies shift depending on the change in naphthyl ring conjugation with the substituent group. In contrast, the modes near 1307 and 1450 cm^{-1} belong to the fluorene stator υ(CC)/δ(CH) mode, and are insensitive to substitution. The low-frequency modes in the region 650-1000 cm^{-1} are very weak in the ground state. However, the most prominent mode in the 690-750 cm^{-1} region corresponds to axle pyramidalisation motion coupled to a H out-of-plane bending (HOOP) (Figure S7).

Excited State Dynamics. The structural evolution of the four motors subsequent to photoexcitation is probed by recording transient absorption and time-resolved Raman spectra

using FSRS. The motors were excited using a femtosecond 'actinic' pump at 400 nm. Transient absorption measurements for all four derivatives at different pump-probe delays show two distinct excited state absorption (ESA) features (see SI Figure S2). The instantaneously generated ESA near 620-800 nm decays in 100-200 fs concomitant with the rise of ESA near 550-620nm. This represents evolution of the FC bright-state to a longer lived (~ps) dark intermediate in all four derivatives.[24] The dark state absorption is increasingly red-shifted and becomes more intense with increasing electronegativity of the substituent. To probe this dark excited state with resonant FSRS, the picosecond Raman pump was tuned in the 560-610 nm window, the resonant wavelength being chosen to yield a similar resonance conditions for all four motors (it is marked by vertical dash arrows in SI Figure S2). The raw FSRS data were background subtracted and corrected for baseline as described in the SI, and are presented in Figure 3.

The processed excited state Raman spectra 200 fs after excitation are presented in Figure3a. The Raman active modes in the excited state are quite broad compared to their ground state counterparts, an effect previously assigned to a distribution of dark state structures.[24] The prominent high frequency modes in R = OMe to H are clearly greatly suppressed when R = CN. Extending the measurements to lower wavenumber, where ground state activity is weak, we observed a broad peak at 720 cm^{-1} in the dark state, which is very weak for the electron donating OMe substituent but strong for electron withdrawing CN. Similarly, a mode at 1170 cm^{-1} is absent for the OMe substituent, but is enhanced in the other derivatives. Figure 3b depicts the change in relative intensity of 720 and 1170 cm^{-1} modes with respect to the 1580 cm^{-1} mode. The peak intensity ratio increases as the substituent changes from –OMe through H and Cl to –CN, i.e. as a function of increasing electron withdrawing character.

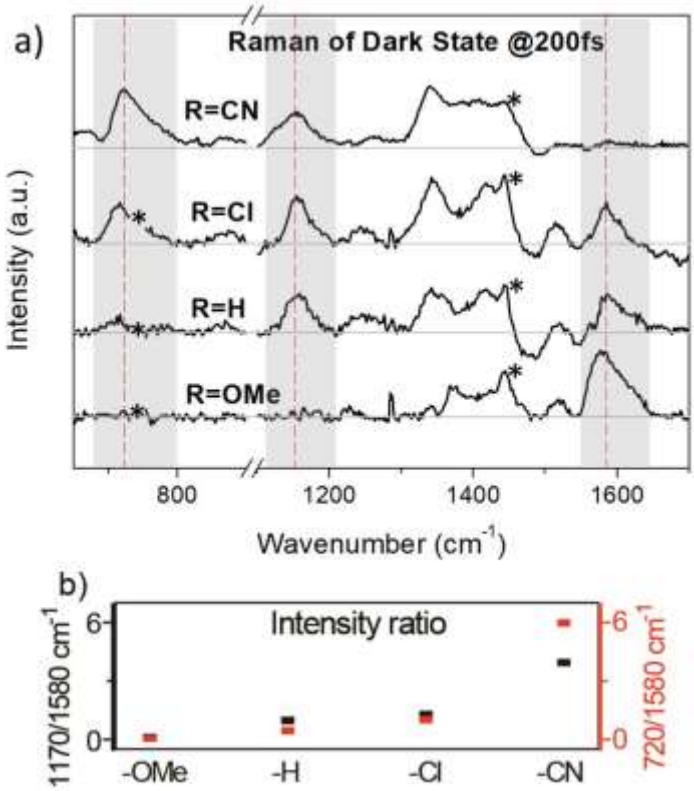

Figure 3: a) Femtosecond stimulated Raman spectra of the dark excited state of molecular motors in methanol, measured at 200 fs pump-probe delay time. Asterisks represents solvent and instrumental artifacts. Grey highlighted area represent region of interest. b) Changes of Raman intensity ratio 1170/1580 cm^{-1} and 720/1580 cm^{-1} as the side-groups are varied.

The broad highest frequency mode at 1580 cm^{-1} in the excited state is assigned to ethylenic C=C + ring stretching on the basis of the ground state DFT calculation. This mode is most intense for the –OMe derivative suggesting the excited state retains strong double bond character. Conversely, this mode is very weak in the –CN derivative, suggesting an excited state geometry in which the ethylenic double bond character is greatly reduced. Instead intense activity in 720 and 1170 cm^{-1} modes is observed, which are themselves weak in the –OMe derivative.

The origin of the enhanced low frequency modes is suggested by earlier quantum chemical calculations of the excited state structure of the fluorene (—H) motors, where the ethylenic carbon on the fluorene ring has changed from sp^2 to sp^3 due to pyramidalization distortion upon formation of the dark state.[23, 25] Note that in all derivatives the pyramidalization mode was calculated at ca 750 cm^{-1} in the ground state (Figure 2) although very weak. In the present case the CN derivative displays an intense low-frequency mode at 720 cm^{-1} and weak mode at 1580 cm^{-1} suggesting that the electron withdrawing character leads to a dark state structure where the pyramidalisation has favored the formation of sp^3 carbon at the ethylenic axle (labeled as an sp^3 dark state, S_{sp3}). Therefore, this strong 720 cm^{-1} mode is assigned to pyramidalisation sp^3 distortion at the axle carbon, and this mode becomes increasingly prominent as the electron withdrawing character of the substituent increases. While not previously reported in motor molecules, such low frequency modes have been seen in other isomerization reactions, in phytochromes and rhodopsins, for example.[26-28] In those cases HOOP activity was an important coordinate, and we note that the calculated ground state pyramidalization mode for the motor molecules also includes significant HOOP displacements (Figure S7). In contrast, in the −OMe derivative the 720 cm^{-1} mode is essentially absent and an intense 1580 cm^{-1} mode is retained, suggesting an excited state geometry where the ethylene axle with sp^2 character carbon (labeled as sp^2 dark state, S_{sp2}) is favored, and there is little displacement along the pyramidalization coordinate. Both the 720 cm^{-1} and 1580 cm^{-1} modes are moderately intense for the –H and –Cl derivatives. This suggests an intermediate structure where both sp^2 and sp^3 geometries are accessible, allowing establishment of a rapid equilibrium between S_{sp2} and S_{sp3}; this overall scheme is illustrated in Figure 4.

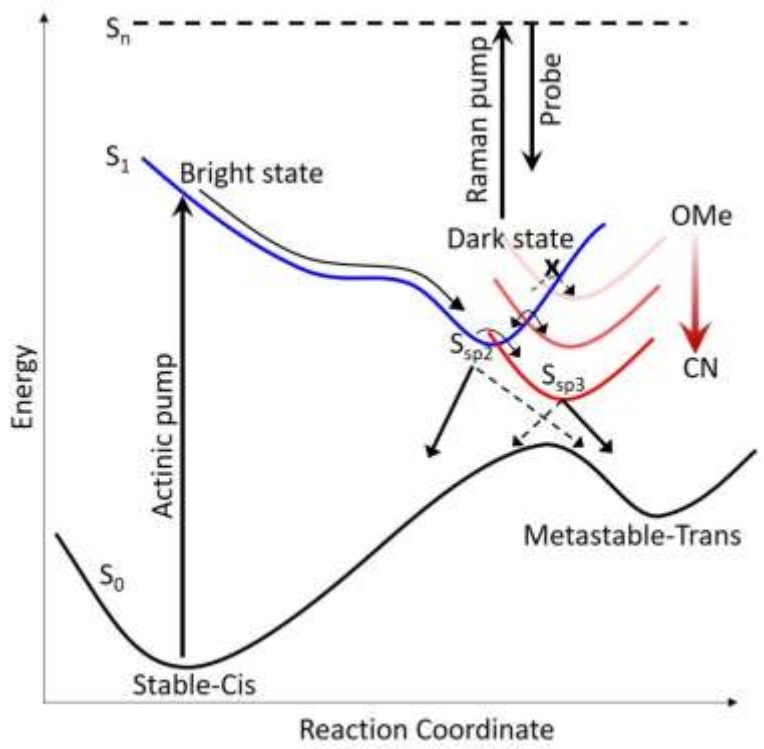

Figure 4: Photophysical model for the photoconversion of second generation molecular motors. The bright state relaxes to the dark state in ca 100 fs.[22] Different populations of S_{sp2} and S_{sp3} states are achieved depending on the nature of substituents, which controls the nature of the nuclear reorganization contributing to the reaction coordinate. The state formed with increasing electron withdrawing character (S_{sp2}, S_{sp2}/S_{sp3} rapid equilibrium, S_{sp3}) influences the probability of the productive isomerization reaction. The 0.5 – 1 ps relaxation dynamics within the dark state (see below) are omitted for clarity.

Excited state Raman spectra thus show that dark excited state structures are substituent dependent: the electron withdrawing −CN derivative has significant sp^3 axle (S_{sp3}) character, while electron donating –OMe derivative has considerable sp^2 axle character, even in the excited state (S_{sp2}). The derivatives with intermediate donating character (–H and –Cl) have intermediate spectra, suggesting that the two excited state structures in fast dynamic equilibrium can 'swing'

on the torsion-pyramidalization coordinate, as reported in spin restricted DFT calculations of motor excited state dynamics.[29] These assignments are represented on the model potential energy surface (Figure 4). Importantly, the observed stabilization of S_{sp3} correlates with a higher conversion efficiency for formation of the ground state metastable product, while S_{sp2} character leads to a low yield of product formation. Therefore, designing molecules that can promote formation of sp^3 axle carbon structures in the excited state should provide higher yield of photoisomerization. We note the short lifetime of S_{sp2} contrasts with the longer lifetime of the S_{sp3} dark state in the −CN derivative. In principle the longer S_{sp3} lifetime itself may lead to higher conversion efficiency – if a competing radiationless process is suppressed for example. However, the present vibrational structure data suggest that it is the structure of the dark state (and therefore the initial structure in the ground state after internal conversion) which determines the yield. For example the −Cl substituent has a short lifetime compared to −CN but a higher yield than −OMe.

The main features of the dark state spectra are independent of delay time (see SI Figure S5), but significant temporal evolution is observed in the ring mode region (1300 – 1400 cm^{-1}) which was also shown to be substituent dependent in ground state spectra (Figure 2). We have plotted the FSRS data for this region in Figure 5a. The data are fit to characterize the evolution by sums of two or three Gaussian functions (shown by blue curves) to resolve underlying peak frequencies and areas; an additional Gaussian function is used to fit the solvent artifact (further fitting details are given in supporting information). The peaks in the range 1330-1375 cm^{-1} are assigned to naphthyl ring υ(CC)/δ(CH) modes (based on our ground state DFT calculation) and undergo a red shift with time as shown by the black vertical dotted line. The peak frequency for this mode is plotted in Figure 5b for all four derivatives. The frequency shifts by 5-10 cm^{-1} on a sub-ps

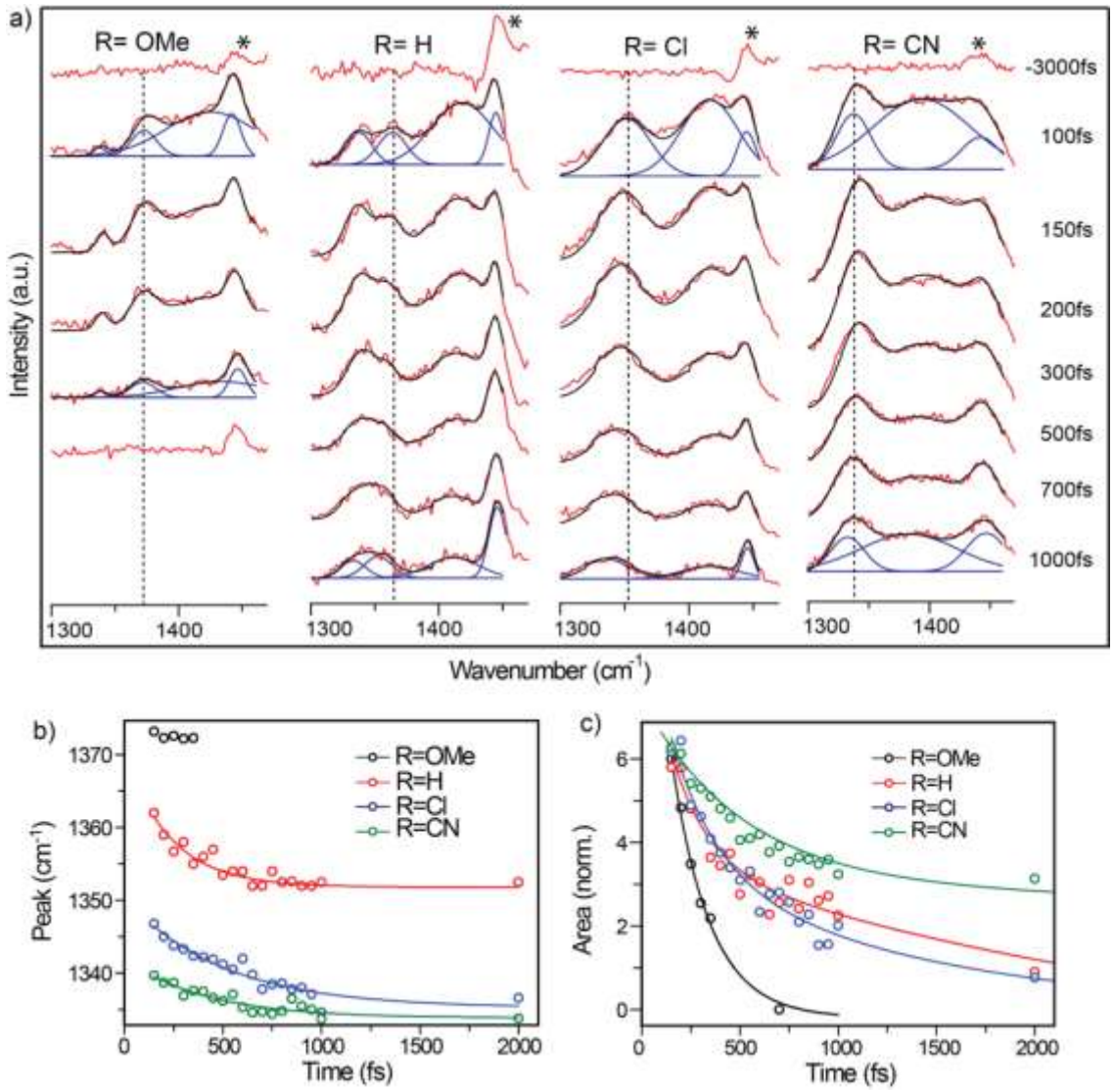

Figure 5: a) Femtosecond stimulated Raman spectra of the molecular motors in the region 1300-1470 cm^{-1} shown at several pump-probe delay times to display spectral shifts (e.g. relative to the black dotted line). Each spectrum (red traces) is fitted by 2 or 3 Gaussian functions (blue curves) to provide a fitted spectrum (black traces). One additional Gaussian function is used to fit the solvent artifacts in the datasets (asterisk marked position) b) The peak frequency shift for 1330-1375 cm^{-1} mode corresponding to naphthyl breathing and c) the associated peak area changes as a function of time, revealing population dynamics.

timescale for the –CN, –Cl and –H derivatives, suggesting structural evolution modifying specifically naphthyl ring modes in the excited state. Other Raman active modes do not undergo peak shifts. Since torsion and pyramidalization in ethylenic isomerization is associated with charge redistribution (sudden polarization) on the ethyleninc bond,[21, 23, 25, 30] the red-shift in the Raman spectra may be explained by stabilization of this new charge distribution. Significantly, transient Raman recorded for the –OMe derivative do not show a shift in peak position for this mode (Figure 5b). This is consistent with −OMe maintaining its double bond S_{sp2} character of the axle. These observations are also correlated with a dynamical peak shift of dark state electronic transient absorption spectra on a ~1 ps timescale for the –CN, –Cl, and –H derivatives, while no significant spectral shift is observed for –OMe (see SI Figure S3).

The dynamics associated with the transient absorption and FSRS spectral shifts, and the non-single exponential FSRS amplitude decay, are tabulated in supporting information. The overall non-single exponential dark state dynamics have been noted previously for the –H derivative and also for first generation motors.[24, 30] The peak area dynamics for this naphthyl ring mode at 1330-1375 cm^{-1} region are plotted in Figure 5c for the four derivatives. The decay is faster for the –OMe derivative and slower for the –CN derivative. This trend correlates with the reported lifetime for dark states from both fluorescence upconversion and transient absorption measurements.[13] Thus, the S_{sp2} dark state for –OMe derivative has a short lifetime (ca 200 fs) and mainly decays to the original ground state. In contrast, the –CN substituted motor has a long-lived (ca. 10ps) S_{sp3} dark state. The relatively long lifetime of the S_{sp3} state in –CN, could be attributed to the larger structural reorganization required to reach the CI.[23] However, The CI accessed from this dark state has a greater probability of forming the metastable product.

In conclusion, we have shown that the structure of the dark excited state of second generation molecular motors varies with the nature of the substituent. More electron withdrawing substituents (–CN) lead to stronger activity in low frequency modes, assigned to formation of an sp^3 axle carbon. Ground state DFT calculations suggest that the 720 cm^{-1} mode can be assigned to the axle pyramidalisation distortion coupled to HOOP motion. For decreasing electron withdrawing character the intensity of these modes and hence population of S_{sp3} dark state decreases and finally, for an electron donating –OMe derivative, the excited state is seen to be trapped in an S_{sp2} state. Importantly, this result correlates with the efficiency of photoconversion in these motors, and aligns with the results of recent existing high quality quantum chemical calculations. It would be instructive if such calculations could be extended to model the measured excited state vibrational spectrum. In addition, we observed 5-10 cm^{-1} peak shift of the rotor breathing modes assigned to stabilization of the charge redistribution in the initial dark state prior to internal conversion via CIs.

Experimental Methods. The synthesis of all derivatives was reported previously.[13, 20] The spectrometers for transient absorption and femtosecond stimulated Raman were described previously,[24] and further details and samples preparation protocols are set out in the supporting information.

Acknowledgements

Financial support was provided by The Netherlands Ministry of Education, Culture and Science (Gravity Program 024.001.035 to WRB, BLF) and the EPSRC (grants EP/R042357/1, EP/J009148/1 to SRM).

Supplementary Information. The supplementary information provides additional detail on steady state and time resolved experiments. Further data is provided on: steady state and transient electronic spectra; time dependent excited state Raman spectra; nuclear displacements associated with the most relevant Raman active ground state vibrational modes, especially the pyramidialization like coordinate; processing procedures for FSRS spectra.

REFERENCES

1. Pollard, M. M.; Klok, M.; Pijper, D.; Feringa, B. L., Rate Acceleration of Light- Driven Rotary Molecular Motors. *Advanced Functional Materials* **2007**, *17*, 718-729.
2. Feringa, B. L., The Art of Building Small: From Molecular Switches to Molecular Motors. *The Journal of organic chemistry* **2007**, *72*, 6635-6652.
3. Feringa, B. L., In Control of Motion: From Molecular Switches to Molecular Motors. *Accounts of chemical research* **2001**, *34*, 504-513.
4. Browne, W. R.; Feringa, B. L., Making Molecular Machines Work. *Nature Nanotechnology* **2006**, *1*, 25-35.
5. Foy, J. T.; Li, Q.; Goujon, A.; Colard-Itté, J.-R.; Fuks, G.; Moulin, E.; Schiffmann, O.; Dattler, D.; Funeriu, D. P.; Giuseppone, N., Dual-Light Control of Nanomachines That Integrate Motor and Modulator Subunits. *Nature nanotechnology* **2017**, *12*, 540.
6. Eelkema, R.; Pollard, M. M.; Vicario, J.; Katsonis, N.; Ramon, B. S.; Bastiaansen, C. W.; Broer, D. J.; Feringa, B. L., Nanomotor Rotates Microscale Objects. *Nature* **2006**, *440*, 163-163.
7. Wang, J.; Feringa, B. L., Dynamic Control of Chiral Space in a Catalytic Asymmetric Reaction Using a Molecular Motor. *Science* **2011**, *331*, 1429-1432.
8. Chiang, P.-T.; Mielke, J.; Godoy, J.; Guerrero, J. M.; Alemany, L. B.; Villagomez, C. J.; Saywell, A.; Grill, L.; Tour, J. M., Toward a Light-Driven Motorized Nanocar: Synthesis and Initial Imaging of Single Molecules. *ACS nano* **2012**, *6*, 592-597.
9. Vicario, J.; Meetsma, A.; Feringa, B. L., Controlling the Speed of Rotation in Molecular Motors. Dramatic Acceleration of the Rotary Motion by Structural Modification. *Chemical communications* **2005**, 5910-5912.
10. Klok, M.; Browne, W. R.; Feringa, B. L., Kinetic Analysis of the Rotation Rate of Light-Driven Unidirectional Molecular Motors. *Physical Chemistry Chemical Physics* **2009**, *11*, 9124-9131.
11. Klok, M.; Janssen, L. P.; Browne, W. R.; Feringa, B. L., The Influence of Viscosity on the Functioning of Molecular Motors. *Faraday discussions* **2009**, *143*, 319-334.
12. Roke, D.; Wezenberg, S. J.; Feringa, B. L., Molecular Rotary Motors: Unidirectional Motion around Double Bonds. *Proceedings of the National Academy of Sciences* **2018**, *115*, 9423-9431.
13. Conyard, J.; Cnossen, A.; Browne, W. R.; Feringa, B. L.; Meech, S. R., Chemically Optimizing Operational Efficiency of Molecular Rotary Motors. *Journal of the American Chemical Society* **2014**, *136*, 9692-9700.
14. Koumura, N.; Zijlstra, R. W.; van Delden, R. A.; Harada, N.; Feringa, B. L., Light-Driven Monodirectional Molecular Rotor. *Nature* **1999**, *401*, 152-155.
15. Kazaryan, A.; Kistemaker, J. C.; Schafer, L. V.; Browne, W. R.; Feringa, B. L.; Filatov, M., Understanding the Dynamics Behind the Photoisomerization of a Light-Driven Fluorene Molecular Rotary Motor. *The Journal of Physical Chemistry A* **2010**, *114*, 5058-5067.
16. Kazaryan, A.; Lan, Z.; Sch√fer, L. V.; Thiel, W.; Filatov, M., Surface Hopping Excited-State Dynamics Study of the Photoisomerization of a Light-Driven Fluorene Molecular Rotary Motor. *Journal of chemical theory and computation* **2011**, *7*, 2189-2199.
17. Briand, J.; Bram, O.; Rehault, J.; Leonard, J.; Cannizzo, A.; Chergui, M.; Zanirato, V.; Olivucci, M.; Helbing, J.; Haacke, S., Coherent Ultrafast Torsional Motion and Isomerization of a Biomimetic Dipolar Photoswitch. *Physical Chemistry Chemical Physics* **2010**, *12*, 3178-3187.

18. Wilcken, R., et al., Complete Mechanism of Hemithioindigo Motor Rotation. *Journal of the American Chemical Society* **2018**, *140*, 5311-5318.
19. Kistemaker, J. C. M.; Stacko, P.; Visser, J.; Feringa, B. L., Unidirectional Rotary Motion in Achiral Molecular Motors. *Nature Chemistry* **2015**, *7*, 890-896.
20. Pollard, M. M.; Wesenhagen, P. V.; Pijper, D.; Feringa, B. L., On the Effect of Donor and Acceptor Substituents on the Behaviour of Light-Driven Rotary Molecular Motors. *Organic & Biomolecular Chemistry* **2008**, *6*, 1605-1612.
21. Filatov, M.; Olivucci, M., Designing Conical Intersections for Light-Driven Single Molecule Rotary Motors: From Precessional to Axial Motion. *The Journal of organic chemistry* **2014**, *79*, 3587-3600.
22. Conyard, J.; Addison, K.; Heisler, I. A.; Cnossen, A.; Browne, W. R.; Feringa, B. L.; Meech, S. R., Ultrafast Dynamics in the Power Stroke of a Molecular Rotary Motor. *Nature chemistry* **2012**, *4*, 547-551.
23. Pang, X.; Cui, X.; Hu, D.; Jiang, C.; Zhao, D.; Lan, Z.; Li, F., "Watching" the Dark State in Ultrafast Nonadiabatic Photoisomerization Process of a Light-Driven Molecular Rotary Motor. *The Journal of Physical Chemistry A* **2017**, *121*, 1240-1249.
24. Hall, C. R.; Conyard, J.; Heisler, I. A.; Jones, G.; Frost, J.; Browne, W. R.; Feringa, B. L.; Meech, S. R., Ultrafast Dynamics in Light-Driven Molecular Rotary Motors Probed by Femtosecond Stimulated Raman Spectroscopy. *Journal of the American Chemical Society* **2017**, *139*, 7408-7414.
25. Li, Y.; Liu, F.; Wang, B.; Su, Q.; Wang, W.; Morokuma, K., Different Conical Intersections Control Nonadiabatic Photochemistry of Fluorene Light-Driven Molecular Rotary Motor: A Casscf and Spin-Flip Dft Study. *The Journal of chemical physics* **2016**, *145*, 244311.
26. Kukura, P.; McCamant, D. W.; Yoon, S.; Wandschneider, D. B.; Mathies, R. A., Structural Observation of the Primary Isomerization in Vision with Femtosecond-Stimulated Raman. *Science* **2005**, *310*, 1006-1009.
27. Dasgupta, J.; Frontiera, R. R.; Taylor, K. C.; Lagarias, J. C.; Mathies, R. A., Ultrafast Excited-State Isomerization in Phytochrome Revealed by Femtosecond Stimulated Raman Spectroscopy. *Proceedings of the National Academy of Sciences* **2009**, *106*, 1784-1789.
28. Roy, P. P.; Abe-Yoshizumi, R.; Kandori, H.; Buckup, T., Point Mutation of Anabaena Sensory Rhodopsin Enhances Ground-State Hydrogen out-of-Plane Wag Raman Activity. *The journal of physical chemistry letters* **2019**, *10*, 1012-1017.
29. Filatov, M.; Olivucci, M., Designing Conical Intersections for Light-Driven Single Molecule Rotary Motors: From Precessional to Axial Motion. *Journal of Organic Chemistry* **2014**, *79*, 3587-3600.
30. Roy, P.; Sardjan, A. S.; Danowski, W.; Browne, W. R.; Feringa, B. L.; Meech, S. R., Photophysics of First-Generation Photomolecular Motors: Resolving Roles of Temperature, Friction, and Medium Polarity. *The Journal of Physical Chemistry A* **2021**, *125*, 1711-1719.